Electronic Shell Structure of Large Metallic Clusters in the Modified Harmonic Oscillator

W.D. Heiss[⋆1] and R.G. Nazmitdinov[⋆⋆]

[⋆] Centre for Nonlinear Studies and Department of Physics
University of the Witwatersrand, PO Wits 2050, Johannesburg, South Africa
[⋆⋆] Bogoliubov Laboratory of Theoretical Physics
Joint Institute for Nuclear Research, 141980 Dubna, Russia

Abstract

Shell structure in the single particle spectrum of deformed harmonic oscillator potentials when a term proportional to $(\vec{L})^2$ is added is analyzed for a large particle number. In the case study presented here it is argued that, in view of the chaotic nature of the problem, a thorough understanding of the classical situation provides essential guidance in tackling the corresponding quantum mechanical problem. A scaling law which gives a dividing line between regular and chaotic behavior in terms of energy, deformation and strength of the $(\vec{L})^2$ term has been found. According to this law, shell structure survives for higher particle numbers only with lesser deformation.

PACS numbers: 05.45.+b, 36.40.Qv, 71.24.+q, 21.10.-k

1 Introduction

Finite Fermi systems give rise to shell structure as is well known from the existence of magic numbers in atoms and nuclei. Nowadays, shell effects are also established in metallic clusters [1, 2, 3]. The first experimental evidence in alkali metallic clusters [4], and independently the theoretical prediction of

[1]heiss@physnet.phys.wits.ac.za

magic numbers within the framework of the spherical jellium model [5, 6], have been major hallmarks in this field.

The valence electrons in metallic clusters are strongly delocalized. They play an essential role in the understanding of many observables and they can be treated by the mean field approach. The jellium model works very effectively for monovalent metallic clusters like sodium and potassium. This mean field model describes a single valence electron that interacts with the average potential which is generated by the other electrons and ions. The structure of the ions is neglected, they are assumed to form a constant positive background or jellium density within a finite volume. While the spherical jellium model has been able to explain general features of enhanced abundances of valence electrons in spherical clusters [7]–[9], it has been recognized that the finer structure in the mass spectra between magic numbers can be explained via symmetry breaking mechanisms [10]–[12] similar to the situation in nuclear physics [13]. A spherically symmetric mean field leads to very strong shell effects which is manifested in the stability of the noble gases, magic nuclei and magic metallic clusters. When a spherical shell is only partially filled, a spontaneous breaking of spherical symmetry can give rise to a deformed equilibrium shape, if it is associated with an energy gain. For clusters with incompletely filled shell, it has been suggested, in analogy with atomic nuclei, to consider a quadrupole deformation which leads to the lifting of the degeneracies in the spherical model. In fact, this idea was implemented by Clemenger [10] who applied the modified harmonic oscillator model (MHO) to metallic clusters where the model played an important role in the understanding of various experimental data (see for review [1, 2]). The MHO with a spin–orbit term was introduced by Nilsson [14] in nuclear physics, and it is a very effective tool in the analysis of ground state deformations and sin-

gle particle excitations for many nuclei [13, 15]. The same model without the spin–orbit term seems to work successfully in reproducing the shapes of small clusters which have been calculated by the more sophisticated methods of quantum chemistry [1]. Based on these results it is therefore accepted that cluster deformations exist. This is in fact confirmed at least for clusters with $A \leq 40$ either by the Clemenger–Nilsson (CN) model or by a self-consistent Kohn–Sham density–functional method [16] (KS) with deformed jellium backgrounds [17]–[20].

Nowadays there is experimental evidence of shells for metallic clusters with more than 1000 atoms [7]–[9],[21, 22]. The shell ground state properties of spherical metallic clusters containing a few thousand valence electrons can be described within the KS approach using the spherical jellium model [23]. Solving the KS equations is quite difficult when deformation effects are taken into account, even for modern supercomputers. It turns out that phenomenological potentials used traditionally in nuclear physics serve a purpose similar to those obtained within the KS approach if the relevant parameters are adjusted appropriately. Typical potentials are the Woods–Saxon (and its various modifications) (WS) and the MHO potential, i.e. the CN model. The main idea of the approach exploiting the WS and the MHO is to use the single particle spectrum generated by the potential to calculate shell energies only, because neither WS nor CN models allow for a description of binding energies for neutral or charged clusters. Following Strutinsky's idea [24], the energy of an interacting Fermi system is divided into a smooth part, denoted by $\tilde{E}$, and an oscillating part which is the shell correction energy denoted by δE, i.e. $E = \tilde{E} + \delta E$. The quantity $\tilde{E}$ varies slowly with particle number and the deformation of the system. In nuclear physics and for metallic clusters it is usually replaced by the liquid drop energy which carries the information

about the bulk properties of the system. The shell correction energy δE contains all the oscillations originating from the bunching of the energy levels. It is obtained by summing the single particle energies of a phenomenological shell model potential and subtracting the average smooth part of the total energy [24, 13, 15].

Using the spherical WS potential for clusters with thousand valence electrons Nishioka *et al* [25] predicted the super-shell phenomenon where the regular oscillations in the level density which reflect the main shells are modulated by an amplitude which oscillates with a lower frequency. Such analysis led to the experimental discovery of the most stable large spherical metallic clusters [21, 22, 3]. Employing the Strutinsky shell correction method, a systematic study of cluster equilibrium shapes has been performed for the WS potential [11, 26] up to 300 atoms and for the MHO potential for clusters with particle numbers up to 300 in [27, 28] and up to 800 in [12]. Effects of deformation are clearly seen in these calculations. For clusters with particle number of up to a few thousand it is natural to use these potentials for the analysis of the existence of deformation. The problem is still being discussed in the ongoing literature (see, for example, discussions by S.Bjørnholm in [3] and [29]).

The equilibrium deformation is ultimately related to the behavior of the shell correction energy δE of the quantum Hamiltonian. According to the periodic orbit theory [30]-[32] (see also [13, 33]) the frequencies in the oscillations of quantum single particle spectra are determined by the corresponding periods of classical closed periodic orbits. The gross shell structure is due to the periodic orbits with a shortest period, whereas the finer details are determined by contributions of longer orbits. This result has been confirmed for spherical potentials used for large clusters [25, 34, 35, 36]. It suggests that

the semi-classical approach can provide deeper insight also into the problem of large deformed clusters by exploiting the tools which have been developed in the study of classical integrable and non-integrable systems.

One of the first attempts to analyze the interplay between shell effects and classical chaotic motion has been done in [37] for an ellipsoidally deformed version of a diffuse nuclear average potential called the Buck-Pilt potential. If the classical problem is non-integrable and displays chaotic behavior, the shell structure of the corresponding quantum spectrum is affected depending on the degree of chaos. More recently these effects were demonstrated for the quadrupole + octupole [38], quadrupole + hexadecapole [39] and for quadrupole + octupole + hexadecapole [40] axial deformed harmonic oscillator potentials.

Initiated by these latter investigations we make use of the connection between ordered motion in the classical problem and shell structure phenomena in the corresponding quantum spectra for phenomenological potentials used for clusters. In practical applications the study of the more realistic deformed WS potential is complicated due to the effective occurrence of many multipoles; this is the subject of a future paper. Since the MHO is being used widely for the interpretation of data [1, 12, 27, 28, 42] we expand in the present paper the preliminary classical analysis of the MHO potential [41] and demonstrate its connection with quantum–mechanical single particle orbitals. One particular result of the classical analysis is a kind of scaling relationship between energy range and the strength λ of the $(\vec{L})^2$ term in the MHO potential. For the corresponding quantum mechanical problem this translates into the finding that pronounced shell structure can occur for increasing particle numbers only for an accordingly decreasing strength λ and/or a decreasing quadrupole deformation.

2 General properties of the model

The level ordering in the WS potential falls between the soft-surface harmonic oscillator (HO) and the hard-surface square well. A similar level ordering is obtained by modifying the HO. The MHO reads in cylindrical coordinates

$$H = \frac{1}{2m}(p_\varrho^2 + p_z^2 + \frac{p_\varphi^2}{\varrho^2}) + \frac{m\omega^2}{2}(\varrho^2 + \frac{z^2}{b^2}) - \lambda\hbar\omega(\vec{L})^2 \qquad (1)$$

where $\vec{L}$ is the angular momentum in units of $\hbar$ and $\lambda > 0$. As the model was originally designed within a pure quantum mechanical context [13, 14] we conveniently use the energy unit $\hbar\omega$ for the $(\vec{L})^2$-term. We consider only axial quadrupole deformations. For $b = 1$ all three components of $\vec{L}$ are conserved because of spherical symmetry; the model becomes then integrable. For $b > 1$ and $b < 1$, which is referred to as prolate and oblate quadrupole deformation, respectively, the problem is non-integrable. The axial symmetry makes the problem a two degrees of freedom system with L_z, denoted classically by p_φ, being a constant of motion.

The classical phase space is unbounded for given energy. The subtraction of a term proportional to the square of the angular momentum allows in principle arbitrarily large values of positions and momenta. This is easily recognized for $b = 1$ where an arbitrarily large value of the then conserved quantity $(\vec{L})^2$ can be given as one of the initial condition; using correspondingly large values of positions and/or momenta, an arbitrary value of the energy can be attained. The corresponding quantum mechanical levels are given by the expression $E_N \approx \hbar\omega l(1 - \lambda l)$ for $n_r = 0\,(N = 2n_r + l)$ for sufficiently large l. For $l > 1/\lambda$ the energy levels are therefore negative. This unboundedness has been dealt with tentatively by adding to the Hamiltonian a term proportional to $\langle N|L^2|N\rangle$. The expectation value is taken with shell

model states and can be expressed in terms of shell numbers [13, 15], if such quantum numbers are well defined which applies to the regular region only. For $b \neq 1$, when $(\vec{L})^2$ is no longer conserved, its time variations extent over a fairly large range of values for generic orbits; depending on initial conditions such values have no bound in principle. We enter the chaotic region and the corresponding quantum mechanical states become mixtures of angular momentum states. As long as the range of such admixtures obeys the inequality $l \leq l_{\rm crit}$ with $\lambda \cdot l_{\rm crit} = 1$ for a given value of λ, the states are not affected by the unboundedness of the Hamiltonian (1). It is discussed below that, for $b > 1$ and the range of λ-values considered, such states give rise to the chaotic nature of the spectrum. In contrast, states with large values of l exceeding $l_{\rm crit}$ are basically regular and do not mix with the former group of states. The latter states give rise to negative energies but are irrelevant for our discussion as they are essentially orthogonal to the former relevant group.

Since the model is non-integrable for $b \neq 1$ and $\lambda \neq 0$ there is no obvious basis for the corresponding quantum mechanical problem. If $\lambda \ll 1$ and $b > 1$ the adequate basis makes use of the asymptotic quantum numbers [43] which diagonalize the Hamiltonian for $\lambda = 0$ (see below). While this approach facilitates the technical problem, even this representation requires great numerical effort to tackle the problem. In accordance with the classical problem, the quantum spectrum shows all characteristics of chaotic behavior for large systems.

We have chosen the upper limit $b = 2$, which is denoted super-deformation for nuclei [15]. Super-deformation seems to exist in metallic clusters, at least for small particle numbers (see, for example [1, 2, 19, 20, 26, 27, 28]). We focus our attention only on $1 < b \leq 2$, since $b < 1$ (oblate case) can

be obtained from the results of the former case by interchanging ϱ and z and suitably replacing ω by $b\omega$. This is in stark contrast with the situation considered in [37, 38, 40]. There the oblate case is chaotic and shell structure is essentially destroyed once higher multipoles are added while shell structure can prevail in the prolate case. Note, that the potential used in [37] contains effectively higher multipoles.

3 Classical treatment

For most of the results presented here it suffices to consider $p_\varphi = 0$ in Eq.(1). Larger values of p_φ are discussed at the end of this section.

We first consider qualitatively the case of spherical symmetry, i.e. $b = 1$. The problem reduces to one degree of freedom since now $p_\theta = m\dot{\theta}r^2 = zp_\varrho - \varrho p_z$ is conserved. Here r and θ refer to the usual polar coordinates. Closed orbits occur if the radial and angular frequencies are commensurate (see, for example [44]). Rewriting Eq.(1) as

$$H = (p_r^2 + p_\theta^2/r^2)/(2m) + m\omega^2 r^2/2 - \lambda\omega p_\theta^2/\hbar \tag{2}$$

we obtain closed orbits if

$$t/s = 1/2 - \lambda p_\theta/\hbar \tag{3}$$

with integers t, s. For instance, when $t/s = 1/3, 1/4, \ldots$ the trajectory forms essentially a triangle, a square *etc.* in the $\varrho - z-$plane; for $t/s = 2/5$ we get the five star, and so forth. The precise shapes of these geometrical figures depend on the magnitude of λ in that small values of λ produce polygons with rounded corners while larger values yield loops at the corners as is illustrated in Fig.(1). The appropriate scaling of λ is given by the kinematical constraint

between the energy and the angular momentum which reads

$$E + \lambda\omega p_\theta^2/\hbar \geq \omega|p_\theta| \tag{4}$$

Here we stress again that for positive values of λ, as used in actual applications, the value of the angular momentum p_θ is not limited in its absolute value for given energy; in particular, if $4\lambda|E| > \hbar\omega$, arbitrarily large positive or negative values may be assumed by p_θ.

For the deformed system, the orbits are Lissajous figures when $\lambda = 0$. Closed orbits are obtained for rational values of b. Our interest is directed towards short periodic orbits. Fig.(2a) displays the phase space structure at $\varrho = 0$ where the surfaces of section are taken. Note that the whole region to the left and right, i.e. outside the lines $z = \pm\sqrt{\hbar/(2\lambda m\omega)}$, is accessible as long as the two lines do not intersect with the ellipse which forms the other part of accessible phase space. If λ is sufficiently large to allow intersection of the lines with the ellipse, the phase space becomes connected. In this case the part of the ellipse which is to the left and right of the lines is inaccessible. In Fig.(2b) surfaces of sections for $\lambda = 0.03$ are given for four different orbits. With the choice of energy $E = 10$ and the frequency $\omega = 1.5$ the two lines are outside the ellipse. (For convenience we use units for which $m = 1$ and $\hbar\omega = 1$). The same pattern is obtained if E and λ are rescaled such that $E\lambda$ =const (see discussion below). The diagram of Fig.(2b) refers to $b = 2$, but the pattern as described prevails for $1 < b \leq 2$. Note that, in accordance with the estimates below, the onset of chaos is discernible just at the periphery of the ellipse, which is the region where E_ϱ (the energy associated with the motion in the ϱ-variable) is small. Typical trajectories of periodic orbits are displayed in Figs.(3); Fig.(3a) corresponds to the black dots on the far right and left of the phase diagram, Fig.(3b) is

the orbit sitting in the centre of the four islands, and Figs.(3c) and (3d) are represented by crosses in Fig.(2b). It was observed in [41] that there is a remarkable similarity between short periodic orbits discussed above and the ones occurring in a WS potential with increasing quadrupole deformation. In fact, the short periodic orbits are of the same geometrical shape and occur in similar regions of the surfaces of section. This similarity could indicate that shell structure effects may be similar for the two potentials. A more careful analysis taking into account stability and degeneracies of corresponding orbits [13, 32] goes beyond the scope of this paper.

For larger values of λ hard chaos takes over quickly within the ellipse, in particular when the two lines enter the ellipse. We make two important observations: (1) regular motion prevails far outside the ellipse which is the whole area to the left of the left line and to the right of the right line. These orbits may attain very large values of ϱ and z; also the variation of the angular momentum p_θ is unlimited in principle. (2) The variation of p_θ ranges typically between -50 and $+50$ for generic orbits inside the ellipse for our choice of parameters. In Figs.(4) we illustrate typical surfaces of section and trajectories for the two cases. The orbit on the bottom left of Fig.(4) is representative for a regular orbit and its surface of section produces the kind of tori lying completely outside the ellipse as illustrated on the top left of Fig.(4); the irregular trajectory on the bottom right of Fig.(4) produces the irregular dots inside and outside the ellipse as shown on the top right; note the proximity to the periphery of the ellipse of the dots outside the ellipse.

The characteristics of these two types of orbits are significant when considering a corresponding quantum mechanical calculation. The nearly regular motion for very large values of p_θ is expected to lead to little mixing of the class of states which is characterized by very large ($l > 60$) and fairly sharp

values of the angular momentum. Also the quantum shell number is still well defined for these states. These are the states which make the quantum mechanical problem unbounded from below. Owing to their negligible mixing to the states discussed in the following they are virtually orthogonal upon the states in the chaotic region. Their classically regular nature is reflected by the *de facto* existence of good quantum numbers. The occurrence of chaos is therefore not the result of unbounded motion, neither classically nor quantum mechanically. However, the other class of states is expected to have not only substantial expectation values of the operator $(\vec{L})^2$ (corresponding to $l \simeq 30$) but in particular a variance of similar magnitude. Consequently, shell structure is expected to be quite weak and the concept of shell quantum number becomes ill defined. There is of course a gradual transition between the two classes. The values given for l refer to $\lambda \leq 0.02$. We note that these physically relevant states obey the criterium $l \cdot \lambda < 1$. The results of the following section fully confirm such expectations.

We conclude the discussion of the classical motion by the results of a perturbative treatment [45] which was successfully employed in [40]. When $b > 1$ we average over the angle θ_ϱ after rewriting the Hamiltonian in terms of action and angle variables of the unperturbed problem. This is sensible as long as the variation of θ_ϱ of the exact motion is faster than that of θ_z, which is ensured if $E_\varrho \gg E_z$, where E_ϱ and E_z are the respective energies residing in the $\varrho-$ and $z-$ motion. In principle, these energies are not constants of motion, but the two degrees of freedom become uncoupled within the approximation. In fact, we obtain after averaging of Eq.(1) the effective Hamiltonian $H_{\rm eff} = H_\varrho + H_z$ with

$$H_\varrho \;=\; \frac{p_\varrho^2}{2m} + \frac{m\omega^2}{2}\varrho^2$$

$$H_z = \alpha(\frac{p_z^2}{2m} + \frac{m\tilde{\omega}_z^2}{2}) \tag{5}$$

where

$$\begin{aligned} \alpha &= 1 - 2\lambda\frac{E_\varrho}{\hbar\omega} \\ \tilde{\omega}_z &= \omega\sqrt{(\frac{1}{b^2} - 2\lambda\frac{E_\varrho}{\hbar\omega})/\alpha} \end{aligned} \tag{6}$$

To ensure a real effective frequency $\tilde{\omega}_z$ in Eq.(6) we read off an inequality which must be obeyed to render the approximation valid. In view of $E \approx E_\varrho$ it may be written as

$$\lambda E < \frac{\hbar\omega}{2b^2}. \tag{7}$$

We note that the exact solutions are perfectly well represented by the motion governed by $H_{\rm eff}$ if the inequalities are observed. We return to the important inequality (7) in the next section.

So far we have concentrated our discussion upon $p_\varphi = 0$ which suffices for low values of p_φ. For larger values the pattern changes, however, in that chaotic motion is suppressed to an increasing extent for increasing values of p_φ. Stable periodic orbits occur for large values of p_φ at λ-values for which the situation is fully chaotic at the lower p_φ-range. An example is illustrated in Fig.(5). These orbits will of course prevail in the corresponding quantum mechanical spectrum, when the full spectrum is considered. We discuss in the next section that such levels can lead to an overestimation of shell effects for the total energy of large clusters.

4 Quantum mechanical treatment

As it was mentioned above for deformed system the obvious basis uses the asymptotic quantum numbers [14, 43] which diagonalize the Hamiltonian for $\lambda = 0$. The boson operators are a_z and $a_z^\dagger$ for the z-motion while for the two dimensional motion perpendicular to the z-direction we use

$$A_\pm = \frac{1}{\sqrt{2}}(a_x \mp i a_y) \tag{8}$$

$$A_\pm^\dagger = \frac{1}{\sqrt{2}}(a_x^\dagger \pm i a_y^\dagger). \tag{9}$$

The conserved z-component of the angular momentum reads in this basis

$$L_z = n_+ - n_- \tag{10}$$

where $n_\pm$ are the occupation numbers referring to the operators $(A_\pm)^\dagger A_\pm$. For a fixed eigenvalue of L_z, denoted by Λ, we effectively have two quantum numbers defining the basis, i.e. n_z and n_+. This reflects the two degrees of freedom of the corresponding classical situation.

The unperturbed ($\lambda = 0$) spectrum is given by

$$E_{n_z,n_+} = \hbar\omega(2n_+ + 1 - \Lambda + \frac{2n_z+1}{2b}) \tag{11}$$

and the square of the angular momentum operator reads

$$\begin{aligned}(\vec{L})^2 &= \frac{1}{2}(\frac{1}{b}+b)((2n_z+1)(2n_+ + 1 - \Lambda) - (a_z^2 + (a_z^\dagger)^2)(D + D^\dagger)) \\ &+ \frac{1}{2}(\frac{1}{b}-b)((a_z^2 + (a_z^\dagger)^2)(2n_+ + 1 - \Lambda) - (D + D^\dagger)(2n_z+1)) \\ &+ (a_z^2 - (a_z^\dagger)^2)(D - D^\dagger) - 1 + \Lambda^2 \end{aligned} \tag{12}$$

where we used the combination $D = A_+ A_-$.

It is now straightforward to set up the matrix of the full Hamiltonian. Parity conservation is reflected by the fact that the problem reduces into even or odd occupation numbers n_z. The occupation numbers n_+ start with the positive value of Λ. We stress that the general form for $(\vec{L})^2$ as given by Eq.(12) mixes states with $\Delta N = 0, 2, 4$ for $b \neq 1$. As a consequence, the calculation cannot be restricted to a particular shell number N for the deformed case as it is usually done in nuclear physics [13, 15]. In particular, the wave functions will be superpositions over a range of shell numbers where the degree of the mixing increases with increasing deformation and/or energy.

From Eq.(11) we conclude that, if one decides to truncate at $n_+^0 = N_+$, the range of n_z must extent up to $N_z = [2b \cdot N_+]$ where [...] denotes the integer part of a given number. With this choice it is ensured that the unperturbed basis is consistently represented up to $E_{\rm cons} = (2N_+ + 1 - \Lambda + 1/(2b))$ (in units of $\hbar\omega = 1$), in other words, all possible degeneracies are taken into account up to $E_{\rm cons}$; for $b = 1$ these degeneracies are just the possible angular momentum values. Note that the range between $E_{\rm cons}$ and $E_{\rm max} = (2N_+ + 1 - \Lambda + (2N_z + 1)/(2b))$ cannot be omitted for reasons of consistency, since n_+ and n_z must run *independently* to their respective maximal values. These considerations are crucial in the present context as the mixing of low lying levels with high angular momenta is essential. It is instructive to discuss first the mixing of angular momenta for $b = 2$ and $\lambda = 0$ where the eigenstates are exactly available. In Table (1) we give the average $\overline{L^2} = \langle n|(\vec{L})^2|n\rangle$ and the variance $\Delta L^2 = \sqrt{\langle n|(\vec{L})^4|n\rangle - (\overline{L^2})^2}$ for some selected positive parity levels for $\lambda = 0$ (recall $\Lambda = 0$ and $\hbar\omega = 1$). Note in particular the large values of the variances which often exceed those of the averages. The switching on of the $(\vec{L})^2$ term not only lifts the degeneracies but brings about a strong mixing among all levels. This becomes obvious in

Table (2) where we display corresponding quantities for $\lambda = 0.01$. The appreciable mixing of high angular momenta signals interaction of many levels on a large scale which is also confirmed by the eigenvectors. For the numbers chosen they pick up typically twenty and more components larger than 0.1 from rather distant unperturbed states, the eigenstates become strongly delocalized. This mechanism requires a considerable extension of the basis in mean field calculations even for relatively small strongly deformed clusters.

The strong mixing between levels, irrespective of the basis chosen, is related to the onset of chaos [46], which is confirmed by the nearest neighbor analysis of the spectrum. A particular sample is illustrated in Fig.(6); a sample average would yield an almost perfect match. This strong result cannot be affected by a volume conservation condition $\omega^2\omega_z = const.$, which is used for the calculation of Potential Energy Surfaces in order to find global and local minima, which yield equilibrium shapes and shape isomers, respectively (see e.g. [20, 27]). In fact, while the effect of this constraint may change the level ordering once the $(\vec{L})^2$ term is included, it is observed (e.g. [15]) that the ellipsoidal shape at large distortion becomes unfavorable for any combination of filled single particle orbitals. In addition, the increased level density at higher energy enhances the interaction of the single particle states. Therefore, there is little scope to find pronounced shell effects for a system with particle numbers that fill shells beyond $N = 4$ in the unperturbed basis and $b \geq 2$. Likewise, for $N > 20$, even a small deformation such as $b \approx 1.1$ does not support shell structure.

The levels listed in Table (2) are selected according to the strength of their eigenvectors being essentially concentrated in the upper fifth of their total length. We have chosen the truncation of n_+ at $N_+ = 22$ which gives a $1035 \cdot 1035$ total matrix size. The states listed have half of their total norm

exhausted within the first 207 components. The spectrum of the states so selected is displayed in Fig.(7a) as a function of λ. In the top right corner we discern a distinctly irregular pattern which is caused by the arbitrary criterion applied to select the states. In fact, in this region the eigenvectors depend very sensitively on the strength λ, since this is the region where level repulsions occur on a large scale. Therefore, states from high lying unperturbed levels will, owing to their coupling to lower lying states, pick up considerable strength (0.5 for our choice) in their first 207 components for a certain window of λ-values while other states will undergo a similar change for a different window of λ-values. In Fig.(7c) we display a section of the same states without connecting the data points. Here it is clearly seen that a few states maintain their identity for increasing λ while the majority of states is submerged in the morass of a chaotic spectrum. To make this point even clearer, a stricter criterion is used in Fig.(7d) where data are given for state vectors which exhaust 80% of their norm in the first 207 components. Obviously, only a few levels survive, in fact about just the ones which mix weakly. Notice the fairly sharp dividing curve between regular and irregular behavior in Fig.(7a) which, according to the previous section, should be given by the scaling law $E\lambda$ =const.

When no selection is made there are many more levels with comparable and even lower energies for $\lambda \geq 0.005$ as is illustrated in Fig.(7b) where the complete spectrum is displayed. These additional states mix to a lesser extent with the ones discussed above. The additional levels come from higher lying unperturbed levels as seen in Fig.(7b) and have even higher angular momentum components. These states are nearly orthogonal to the states belonging to the chaotic spectrum; they correspond to the states discussed in the previous section and form the space giving rise to the negative part

of the energy spectrum. As a function of λ the energies come down owing to the negative $(\vec{L})^2$-term; accordingly, the corresponding eigenvectors have their bulk components at higher labels. They are the quantum mechanical counterpart of the type of classical orbits displayed on the left column of Fig.(4). Traditionally these states are pushed up in their energy by the *ad hoc* adding of the mean value of L^2 which is, for small deformation, a simple expression in the shell number [10, 27]. This remedy does not affect the eigenvectors, it would change the spectrum but not its statistical properties. The basic reason for this to hold is the fact that the states whose energies tend to minus infinity do not couple with the physically relevant states as the irrelevant states have very large angular momentum while the relevant states have a mixture of only moderate angular momenta. Since the concept of shell numbers breaks down, the mean value of L^2 can no longer be expressed in terms of a shell number and adding it to the spectrum becomes doubtful. On the basis of our findings we rather ignore the irrelevant states.

For completeness we report corresponding results for $b = 1.1$. In Table (3) we present results for $\lambda = 0.1$. To demonstrate the only slightly broken symmetry for the near spherical case this value is chosen much larger than the one usually applied in either nuclear physics or metallic clusters. As a result, irrelevant states with large mean values of angular momentum ($l > l_{\rm crit} = 1/\lambda$) have negative energies. All states are fairly good eigenstates of angular momentum with much smaller spreading ΔL^2 as is expected for this mild deviation from unity of b. In most cases the expectation value of $(\vec{L})^2$ is very close to an eigenvalue $l(l+1)$, we have indicated the corresponding l-values in brackets. The eigenvectors are fairly well localized, there is only limited mixing. A near Poisson distribution is found for the nearest neighbor distribution indicating the near-integrability of the $b = 1.1$ case.

Note, however, that these statements are limited to about the first three hundred levels.

Based upon the inequality $E_z \ll E_\varrho$ we obtain from Eq.(7) the border line $E\lambda \simeq 1/(2b^2)$ between regular motion and expected chaos. A similar dividing line should be expected for the quantum mechanical problem. It appears that the relation $E\lambda \simeq 1/(4b^2)$ can serve as an empirical dividing line between order and chaos as long as $b > 1$. The difference between Eq.(7) and the empirical quantum mechanical result is due to the approximation; also, such border lines are not expected to coincide exactly for the classical and quantum mechanical case. We may combine this relation with $E \approx l(1 - \lambda l)$ ($n_r = 0, \hbar\omega = 1$, N and l sufficiently large) to obtain the estimate $\lambda l \simeq 1/2$ as a border line at around $b = 1$. Therefore, values of l and λ which obey the condition $1/2 \leq \lambda \cdot l \leq 1$ correspond to chaotic motion. (Note that, since outside the chaotic region the values of the angular momentum are almost sharp, values of l can be used to delineate different regions even though it is a dynamical variable.) As a consequence, the values used for λ in nuclear physics, when applied for large metallic clusters, lead to a strong mixing of levels at the high end of the spectrum (see Fig.(7a,7b)) even for values of b close to unity. Hence, shell structure is expected to be weakly pronounced for a large particle number even for mild deformation. For $b = 2$ the emerging shell structure is confined to the very low end of the spectrum and to rather small values of λ.

The results found for the specific examples $b = 1.1$ and $b = 2$ do not change for negative parity states or for $\Lambda > 0$. The spectrum for larger values of Λ nicely slots in with the spectrum for $\Lambda = 0$ to produce typical shell structure as long as b is close to unity. At the end of Section 3 we pointed out that a regular pattern begins to emerge for very large values of

p_φ even when $b = 2$. Note also that, for large values of Λ (the quantum mechanical value of p_φ), $(\vec{L})^2$ becomes diagonally dominant as seen from Eq.(12) thus leading to lesser pronounced level repulsion in line with the increasingly regular classical situation. While levels of large Λ are submerged in the morass of a chaotic spectrum pertaining to lower Λ-values, they are expected to yield discernible shell structure in a Strutinsky type analysis. In calculations by [12, 28], levels belonging to rather high shells occur below the Fermi surface and have to be taken into account in the Strutinsky averaging procedure; pure oscillator states ($\lambda = 0$) are used for the upper part of the spectrum. Even for relatively small clusters with sizes up to $A = 270$ atoms [28] the convergence criterium for the Strutinsky's shell correction method [24] required inclusion of spherical shell numbers up to $N = 16$. In essence, the occurrence of large Λ is associated with very high shell numbers, a region where the applicability of the model is no longer certain. For example, in [12] it was found that for large spherical clusters ($A = 676$ and 832) the energy minima are more pronounced than in the KS calculations, which is an artifact. In other words, while in the axial MHO potential the re-emergence of order and hence shell structure is a fact for large Λ, its physical impact cannot be assessed from this model alone. Moreover, even small non-axial deformations, which are discernible for small clusters [27, 28], will destroy shell effects for large clusters, since L_z is no longer a constant of motion, i.e. Λ is no longer a good quantum number.

5 Summary

Using the classical analysis of single particle motion in the MHO potential our attention is focused on the distinction of regions in phase space of predomi-

nantly regular or chaotic motion, when the deformation b and the term $(\vec{L})^2$ act simultaneously. Important similarities, not obvious at first glance, with regard to the shortest periodic orbits which define the gross shell structure of the single particle spectrum in the MHO potential and in the Woods-Saxon potential have been found previously [41] . Typical trajectories of periodic orbits are displayed in Fig.(3). Both cases give rise to chaotic motion when the deformation in the Woods–Saxon and the $(\vec{L})^2$-term in the MHO potential are turned on. The chaotic behavior is of lesser significance, as long as the interest is focused only on the lower end of the spectrum and the deformation is fairly mild, that is for small metallic clusters. For large metallic clusters, however, with the much larger particle numbers, a higher range of the spectrum becomes relevant; depending on the deformation, chaotic behavior may well interfere with the search for shell structure in this region.

Regular and chaotic behavior are essentially separated by the curve $E\lambda \simeq \hbar\omega/(4b^2)$. When $b > 1$ and $\lambda = 0$, the problem is regular and so is the variation of the classical angular momentum; in fact the variation is determined by the frequencies ω and ω/b. If λ is switched on, the variation becomes quickly irregular, but more importantly, the range of variation increases considerably with increasing λ as it should be expected, since the term $\lambda(\vec{L})^2$ adds angular momentum. In quantum mechanics, switching on the $(\vec{L})^2$ term not only lifts the degeneracies but brings about a strong mixing among all levels of the unperturbed basis. Therefore, the unavoidable truncation of the basis in such a situation must be handled with great circumspection to avoid the occurrence of spurious shell structure. While it is common wisdom that questions of truncation are delicate, we stress that the classical finding, which is the large fluctuation of the angular momenta, provide essential guidance to the problem of the truncation.

From Figs.7 and from the relation $E\lambda \simeq 1/(4b^2)$ ($\hbar\omega = 1$) we conclude that shell structure is possible at higher energies (larger number of particles) only for accordingly small values of λ. For $\lambda \geq 0.007$ (which is smaller by one order of magnitude than the typical ones) and $b = 2$ hard chaos occurs already for $E \geq 10$ which is seen from the Wigner distribution of the nearest neighbor statistic. Shell structure is retrieved for lesser deformation at the same values of energy and λ. One of the basic conclusions of our analysis is that using the MHO model for metallic clusters with a coupling strength λ similar to that in nuclear physics would conflict, at least for larger deformations b, with observation of shell structure. Within the model considered we may speculate that large particle systems tend to restore the near-spherical symmetry to allow for shell structure which basically means increased stability for the appropriate particle number. There seem to be indications to this effect in calculations of the equilibrium shapes for sodium clusters with $A \leq 300$ (see, for example [28]) using the MHO. We conclude that the MHO potential cannot yield shell structure for $b \geq 2$ and shell number larger than about 4, or $b \simeq 1.1$ and shell number larger than about 20. Energy minimization is therefore expected to yield decreasing deformation for increasing particle number.

When the model was introduced originally in nuclear physics [14], neither the unbounded motion nor the inherent chaotic nature was of interest. The $(\vec{L})^2$ term has been introduced to modify the nuclear potential with an effective A-dependence. Its chaotic nature was masked at the time, since only $A \leq 200$ was of interest. The transfer of a well established nuclear structure model to the new physical situation of metallic clusters requires a re–assessment of the phenomenological model, since it entails systems of a considerably larger number of particles, where even a moderate deforma-

tion can have a pronounced effect. The connection between shell structure phenomena in the quantum mechanical spectrum and ordered motion in the analogous classical case leads to the conclusion that the model is useful but only in a restricted domain. Our analysis shows that the two aspects, the unboundedness and chaotic motion, are independent of each other. In fact, the regular classical motion for large values of $(\vec{L})^2$ ($l > l_{\rm crit} = 1/\lambda$) gives rise to quantum mechanical states which have virtually sharp values of l and are essentially orthogonal upon the chaotic states which, in turn, are characterized by the inequality $1/2 \leq l\lambda \leq 1$. The other regular part of the spectrum which is displayed in Fig.7 is obtained for $l\lambda < 1/2$.

The inclusion of higher multipoles into the potential for large system cannot change this finding. The chaotic nature inferred by adding the term $(\vec{L})^2$ destroys the shell structure which is produced in a subtle way by the octupole deformation when added to the quadrupole deformed HO [38]. The hexadecapole deformation, when added to the quadrupole deformed HO, induces shell structure with a pattern similar to that of a lesser deformed quadrupole HO [39]. And the combination yields shell structure for specific values of the octupole and hexadecapole strength [40]. Since the $(\vec{L})^2$ term dissolves all bunching of levels in a deformed potential at higher energies, i.e. for large particle numbers, shell structure can be restored only for a near spherical shape. This property is shared with the effect of the hexadecapole term mentioned above. In fact, similarities between the two terms have been pointed out in [13]. Other shapes of potentials [26] seem to indicate that adding higher multipoles gives rise to shell structure for large particle numbers. It is a challenge to understand such claims in terms of periodic orbits. Work towards this aim is in progress.

This project has been supported by the Foundation for Research Development of South Africa.

References

[1] W.A. de Heer, Rev. Mod. Phys. 65 (1993) 611.

[2] M. Brack, Rev. Mod. Phys. 65 (1993) 677.

[3] Comments At.Mol.Phys. 31, Nos. 3-6 (1995)

[4] W.D. Knight, K. Clemenger, W.A. de Heer, W.A. Saunders, M.Y. Chou, M.L. Cohen, Phys.Rev.Lett. 52 (1984) 2141.

[5] W. Ekardt, Phys.Rev. B 29 (1984) 1558.

[6] D.E. Beck, Solid State Commun. 49 (1984) 381.

[7] S. Bjørnholm, J. Borggreen, O. Echt, K. Hansen, J. Pedersen, H.D. Rasmussen, Phys. Rev. Lett. 65 (1990) 1627.

[8] C. Brechignac, Ph. Cahuzac, F. Carlier, M. de Frutos, J. Leygnier, J.Chem.Phys. 93 (1990) 7449.

[9] T.P. Martin, S. Bjørnholm, J. Borggreen, C. Brechignac, Ph. Cahuzac, K. Hansen, J. Pedersen, Chem. Phys. Lett. 186 (1991) 53.

[10] K. Clemenger, Phys. Rev. B 32 (1985) 1359.

[11] S. Frauendorf, V.V. Pashkevich, Z. Phys. D 26 (1993) S98.

[12] S.M. Reimann, M. Brack, K. Hansen, Z.Phys. D 28 (1993) 235.

[13] A. Bohr, B.R. Mottelson, Nuclear Structure, Vol.2. (Benjamin, New York, 1975).

[14] S.G. Nilsson, Mat.Fys.Medd.Dan.Vid.Selsk. 29 (1955) 16.

[15] S.G. Nilsson, I. Ragnarsson, Shapes and Shells in Nuclear Structure. (Cambridge University Press, Cambridge, 1995).

[16] W. Kohn, L.J. Sham, Phys. Rev. 140 (1965) 1133A.

[17] W. Ekardt, Z. Penzar, Phys.Rev. B 38 (1988) 4273; Z. Penzar, W. Ekardt, Z.Phys. D 17 (1990) 69.

[18] G. Lauritsch, P.-G. Reinhard, J. Meyer, M. Brack, Phys.Lett. A 160 (1991) 179.

[19] Th. Hirschmann, M. Brack, J. Meyer, Ann.Physik (Berlin) 3 (1994) 336.

[20] B. Montag, Th. Hirschmann, J. Meyer, P.-G. Reinhard, M. Brack, Phys.Rev. B 52 (1995) 4775.

[21] J. Pedersen, S. Bjørnholm, J. Borggreen, K. Hansen, T.P. Martin, H.D. Martin, Nature (London) 353 (1991) 733.

[22] C. Brechignac, Ph. Cahuzac, F. Carlier, M. de Frutos, J.Ph. Roux, Phys.Rev. B 47 (1993) 2271.

[23] O. Genzken, Mod.Phys.Lett. B 7 (1993) 197.

[24] V.M. Strutinsky, Sov.J.Nucl.Phys. 3 (1967) 449; Nucl.Phys. A 95 (1967) 420; *ibid* A 122 (1968) 1.

[25] H. Nishioka, K. Hansen, B.R. Mottelson, Phys. Rev. B 42 (1990) 9377.

[26] S. Frauendorf, V.V. Pashkevich, Ann.Physik (Berlin) 5 (1996) 34.

[27] C.Yannouleas, U. Landman, Phys. Rev. B 51 (1995) 1902.

[28] S.M. Reimann, S. Frauendorf, M. Brack, Z.Phys. D 34 (1995) 125.

[29] A. Bulgac, C. Lewenkopf, Phys.Rev.Lett. 71 (1993) 4130.

[30] M.C. Gutzwiller, J.Math.Phys. 12 (1971) 343.

[31] R. Balian, C. Bloch, Ann.Phys. (N.Y.) 69 (1972) 76.

[32] V.M. Strutinsky, A.G. Magner, Sov. J. Part. Nucl. 7 (1976) 138.

[33] M. Brack, R.K. Bhaduri, Semiclassical Physics. (Addison-Wesley Publishing Company, Inc. 1997).

[34] J. Mansikka–ako, M. Manninen, H. Nishioka, Phys. Rev. B 48 (1993) 1837.

[35] J. Lerme, Ch. Bordas, M. Pellarin, B. Baguenard, J.L. Vialle, M. Broyer, Phys. Rev. B 48 (1993) 9028.

[36] N. Pavloff, S.C. Creagh, Phys. Rev. B 48 (1993) 18164.

[37] R. Arvieu, F. Brut, J. Carbonell, J. Touchard, Phys.Rev. A 35 (1987) 2389.

[38] W.D. Heiss, R.G. Nazmitdinov, S. Radu, Phys. Rev. Lett. 72 (1994) 2351; Phys. Rev. B 51 (1995) 1874.

[39] W.D. Heiss, R.G. Nazmitdinov, S. Radu, Phys. Rev. C 52 (1995) R1179.

[40] W.D. Heiss, R.G. Nazmitdinov, S. Radu, Phys. Rev. C 52 (1995) 3032.

[41] W.D. Heiss, R.G. Nazmitdinov, Phys. Rev. Lett. 73 (1994) 1235.

[42] J.G. Eaton, L.H. Kidder, H.W. Sarkas, K.M. McHugh, K.H. Bowen, in *Nuclear Physics Concepts in the Study of Atomic Cluster Physics*, edited by R. Schmidt *et al*, Lecture Notes in Physics vol. 404, p.291. (Berlin, Springer, 1992).

[43] B.R. Mottelson, S.G. Nilsson, Nucl.Phys. 13 (1959) 281.

[44] L.D. Landau, E.M. Lifshitz, Mechanics. (Pergamon Press, Oxford, 1976).

[45] A.J. Lichtenberg, M.A. Lieberman, Regular and Stochastic Motion. (Springer, New York, 1983).

[46] M.C. Gutzwiller, Chaos in Classical and Quantum Mechanics. (Springer, New York, 1990)

n	E_n	$\overline{L^2}$	ΔL^2
1	1.25	0.25	1.35
2	2.25	5.25	5.73
3	3.25	10.3	11.5
4	3.25	2.75	4.85
5	4.25	17.8	15.7
6	4.25	15.3	17.3
7	5.25	32.8	29.1
8	5.25	20.3	23.1
9	5.25	5.35	8.78
17	8.25	80.3	70.7
18	8.25	77.8	69.9
19	8.25	42.7	38.2
20	8.25	35.3	40.6
26	10.25	130	115
27	10.25	113	99
28	10.25	108	97
29	10.25	56	50
30	10.25	45	52
⋮	⋮	⋮	⋮

Table (1). Average values and variances of the operator $(\vec{L})^2$ for a few low energy states for $b = 2$ and $\lambda = 0$.

n	E_n	$\overline{L^2}$	ΔL^2
1	1.25	0.29	1.47
2	2.19	5.85	6.51
3	3.12	13.3	14.7
4	3.22	2.82	5.24
5	4.04	24.0	28.9
6	4.06	18.7	16.3
7	4.85	43.8	47.3
8	4.96	37.0	39.7
9	5.19	6.41	9.80
13	5.91	32.3	36.6
14	6.25	1657	1862
15	6.30	2163	1973
16	6.50	1947	1963
27	7.76	51.3	117
28	7.93	1504	1740
29	7.95	1413	1810
30	8.13	836	1479
⋮	⋮	⋮	⋮

Table (2). Same as Table (1) but for $\lambda = 0.01$.

n	E_n	$\overline{L^2}$	(l)	ΔL^2
1	-28.1	506	(22)	9.6
2	-21.5	420	(20)	9.0
3	-19.5	420	(20)	9.9
4	-15.6	342	(18)	8.4
9	-6.7	272	(16)	9.7
10	-6.2	210	(14)	7.4
17	-0.17	110	(10)	6.7
18	1.1	156	(12)	8.7
20	1.45	0.01	(0)	0.2
21	1.87	71.6	(8)	6.9
22	1.89	110	(10)	7.6
23	2.7	6.7	(2)	4.4
24	2.9	39	(6)	10.5
25	3.0	156	(12)	9.7
26	3.3	22.8	(4)	8.5
27	3.4	0.2	(0)	1.7
⋮	⋮	⋮	⋮	⋮

Table (3). Same as Table (1) but for $b = 1.1$ and $\lambda = 0.1$. Note that for this small deformation the levels are nearly good eigenstates of $(\vec{L})^2$ with averages close to $l(l+1)$ and small variances.

Figure Captions

Fig.1 Typical simple periodic orbits for $b = 1$. The orbits with the loops at the corners are for $\lambda \gtrsim \hbar\omega/(4E)$ while the other two are for $\lambda = \hbar\omega/(25E)$.

Fig.2 Surfaces of section in the plane $\varrho = 0$. In (a) the dependence on λ of accessible phase space (shaded) is illustrated; left: $\lambda < \hbar\omega/(4E)$, right: $\lambda > \hbar\omega/(4E)$. In (b) four orbits of different initial conditions are displayed for $\lambda < \hbar\omega/(4E)$.

Fig.3 Typical short periodic orbits in the $\varrho - z-$plane. Reference to Fig.2 is made in the main text. Figs.(c) and (d) are self-tracing orbits.

Fig.4 Two orbits for the same choice of parameters ($b = 2, \lambda = 0.01$). The left hand column displays the surface of section and the corresponding orbit for a regular orbit while the right hand column gives the respective plots for a typical chaotic orbit.

Fig.5 Two orbits for the same choice of parameters and initial conditions but for different values of p_φ. The left hand column displays the surface of section at $\varrho = 8$ and the corresponding orbit for a regular orbit at $p_\varphi = 61$ while the right hand column gives the respective plots for a typical chaotic orbit at $p_\varphi = 1$.

Fig.6 A nearest neighbour distribution of the unfolded spectrum for $b = 2$ and $\lambda = 0.01$.

Fig.7 (a) Lower end (about 6% of all levels) of the energy spectrum in units of $\hbar\omega$ as a function of the strength λ for states whose eigenvectors exhaust 50% of the norm in the first fifth of the total length. The dividing line $E\lambda = 1/(4b^2)$ can be nicely discerned. (b) Lower end of the spectrum for all levels. (c) A section of (a). (d) Same as (c) but only for states whose eigenvectors exhaust 80% of the norm in the first fifth of the total length.

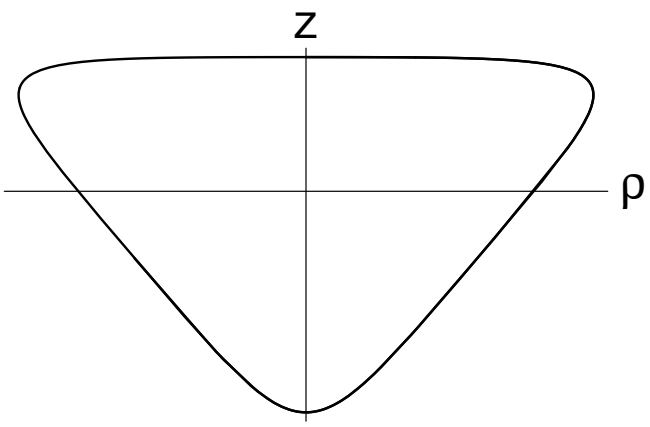
z
ρ

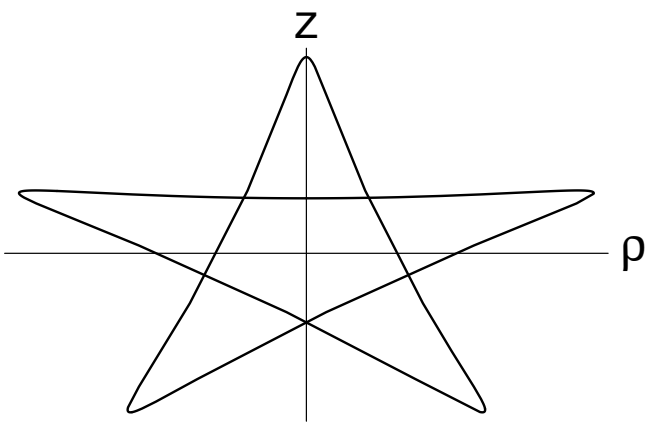
z
ρ

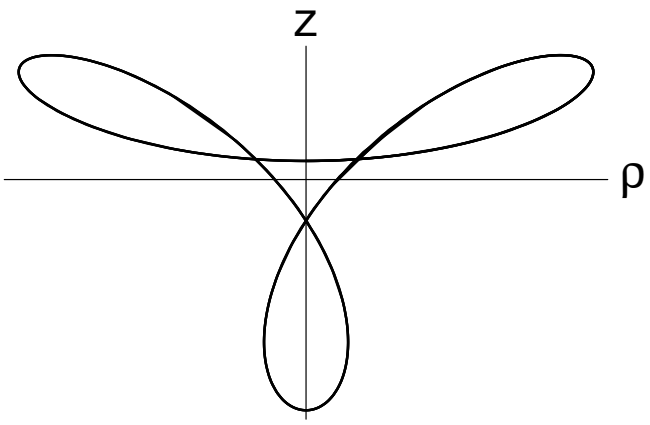
z
ρ

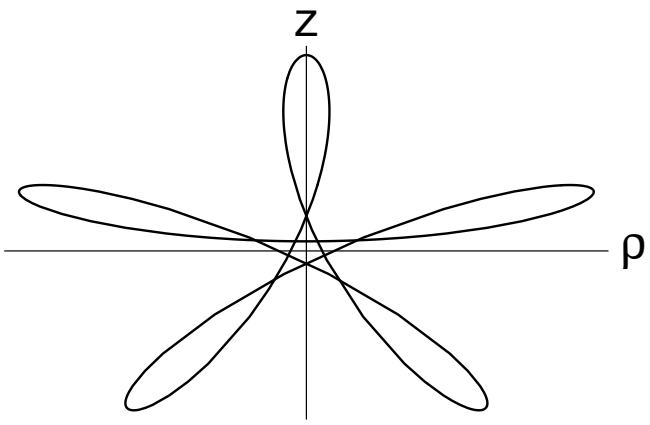
z
ρ

(a)

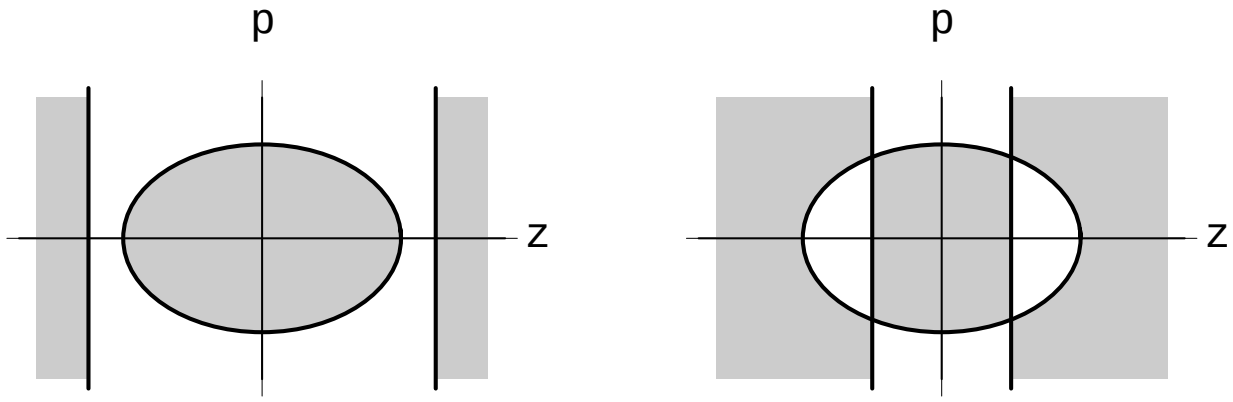

(b)

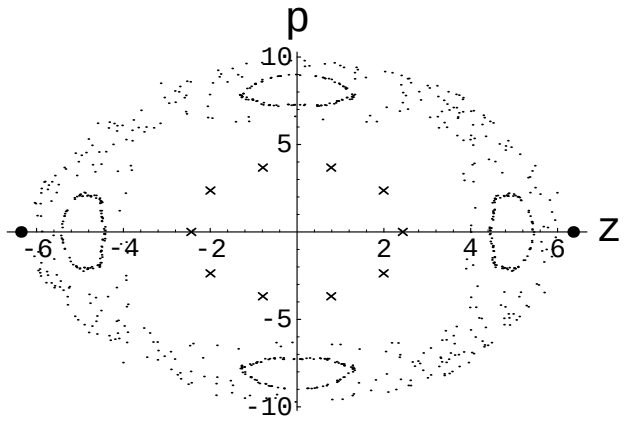

(a)

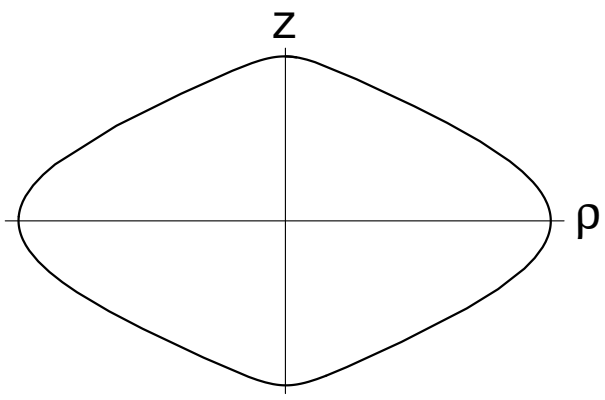

(b)

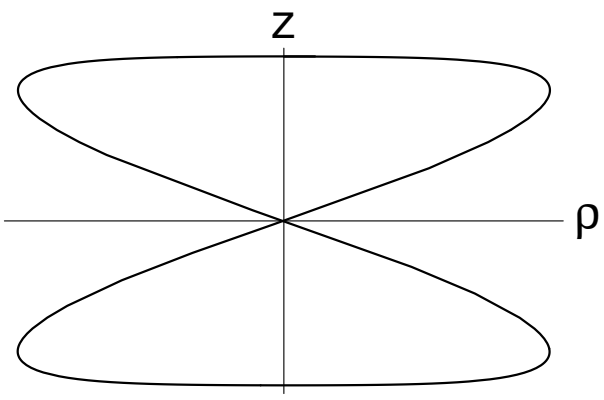

(c)

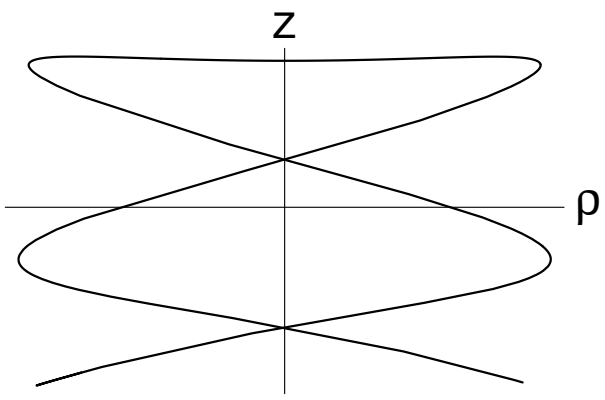

(d)

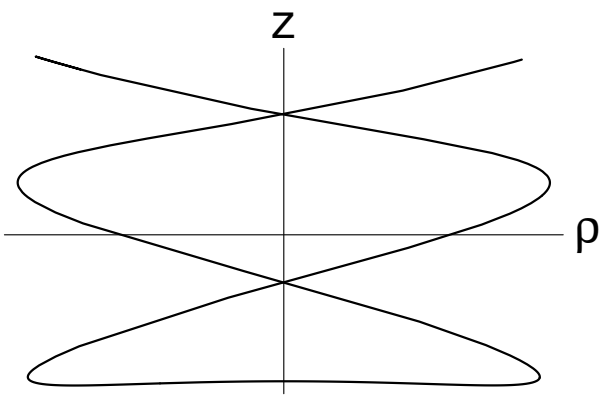

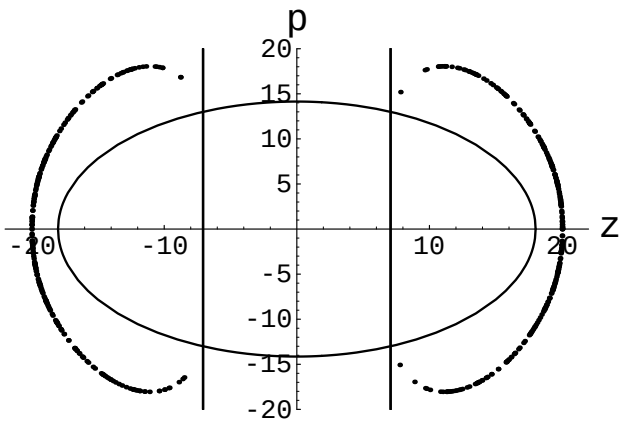
p
z
20
15
10
5
-5
-10
-15
-20
-20
-10
10
20

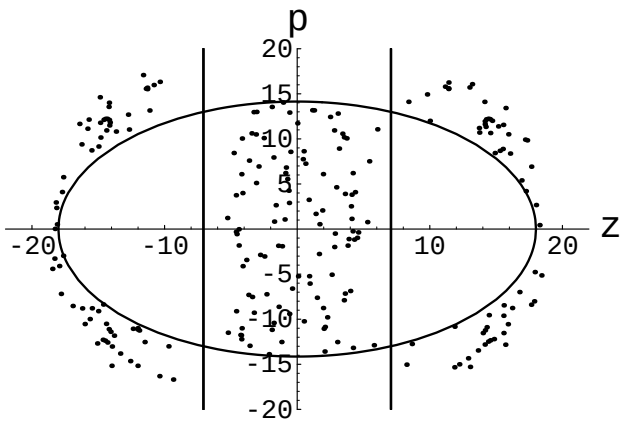
p
z
20
15
10
5
-5
-10
-15
-20
-20
-10
10
20

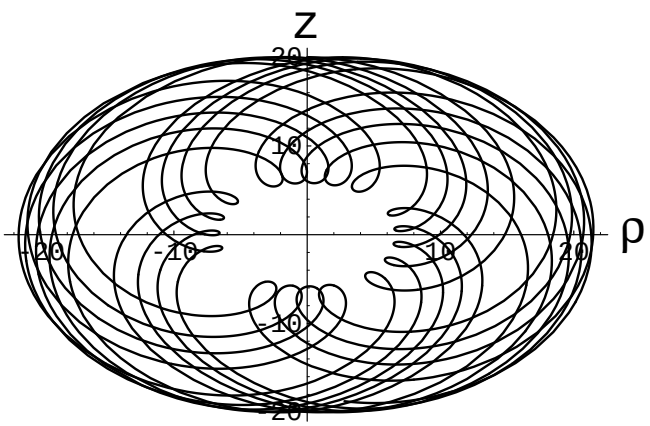
z
ρ
20
10
-10
-20
-20
-10
10
20

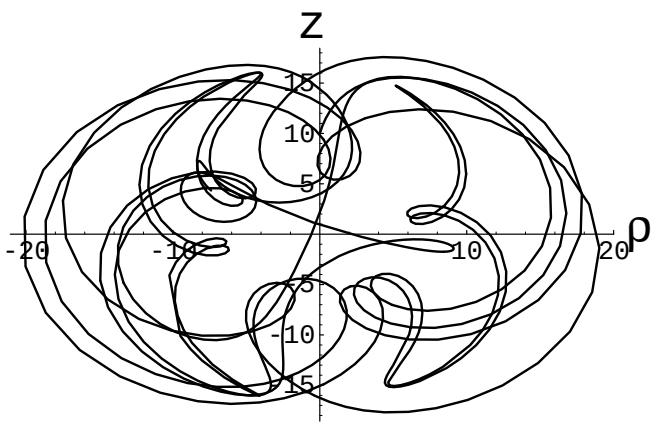
z
ρ
15
10
5
-5
-10
-15
-20
-10
10
20

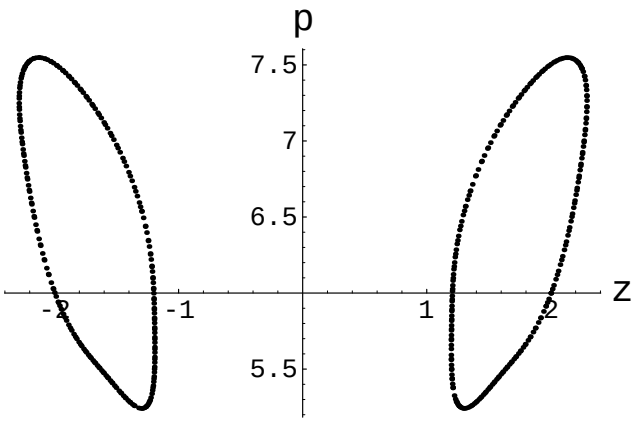
p
7.5
7
6.5
5.5
-2
-1
1
2
z

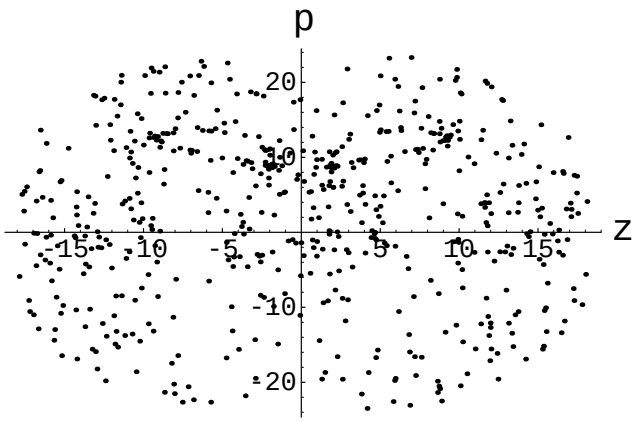
p
20
10
-10
-20
-15
-10
-5
5
10
15
z

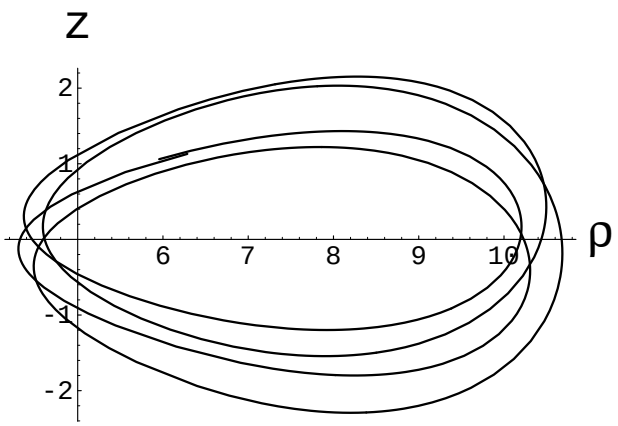
z
2
1
-1
-2
6
7
8
9
10
ρ

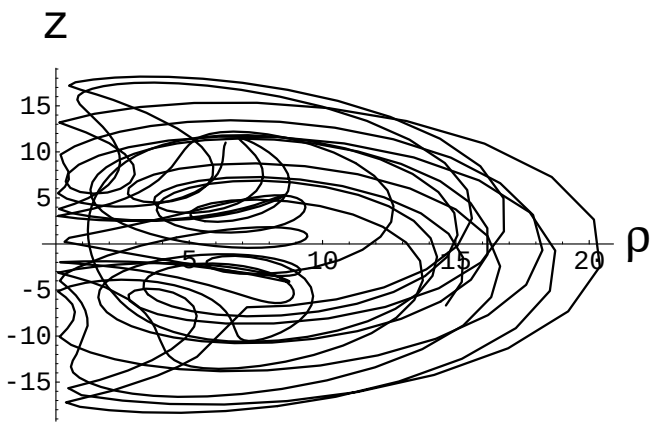
z
15
10
5
-5
-10
-15
5
10
15
20
ρ

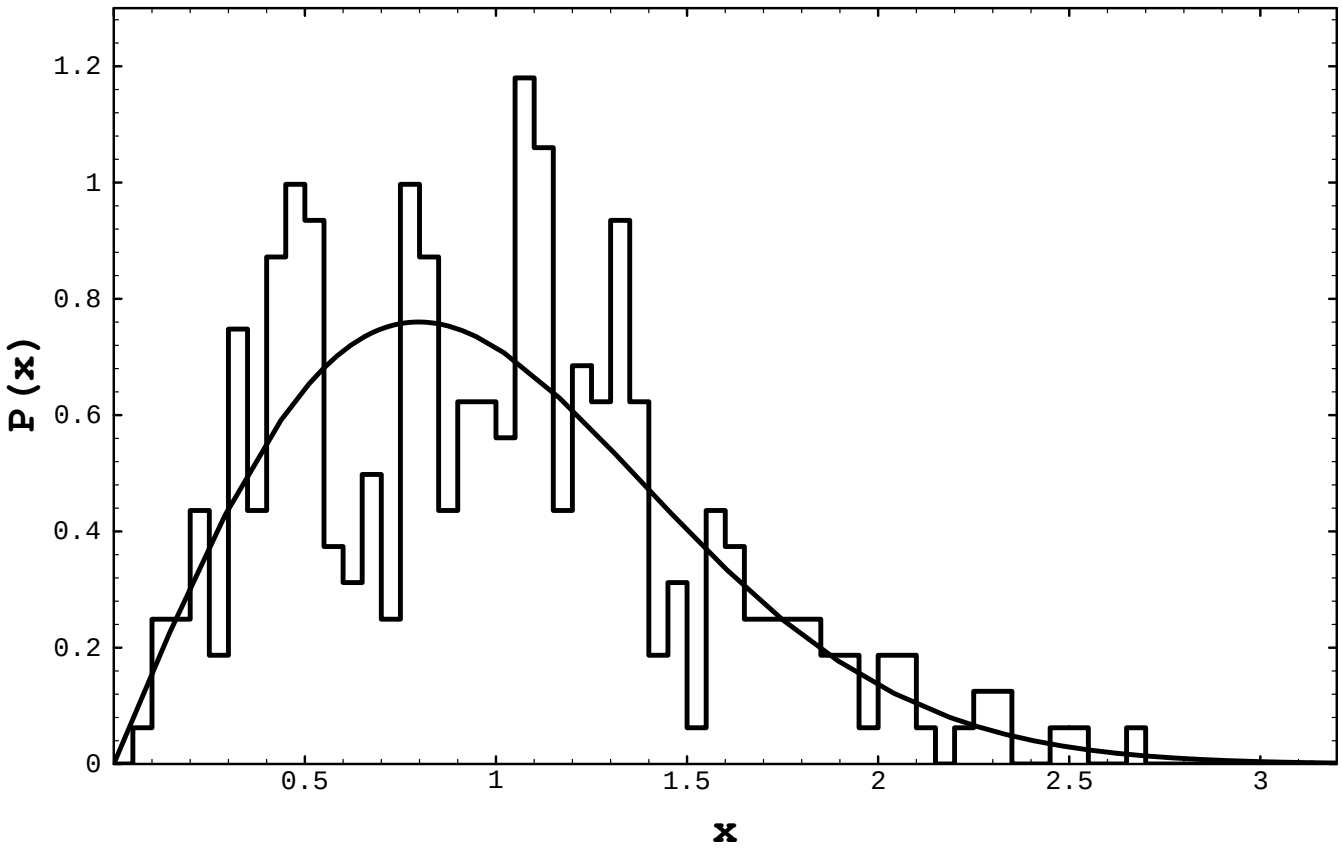
P(x)
x
0
0.2
0.4
0.6
0.8
1
1.2
0.5
1
1.5
2
2.5
3

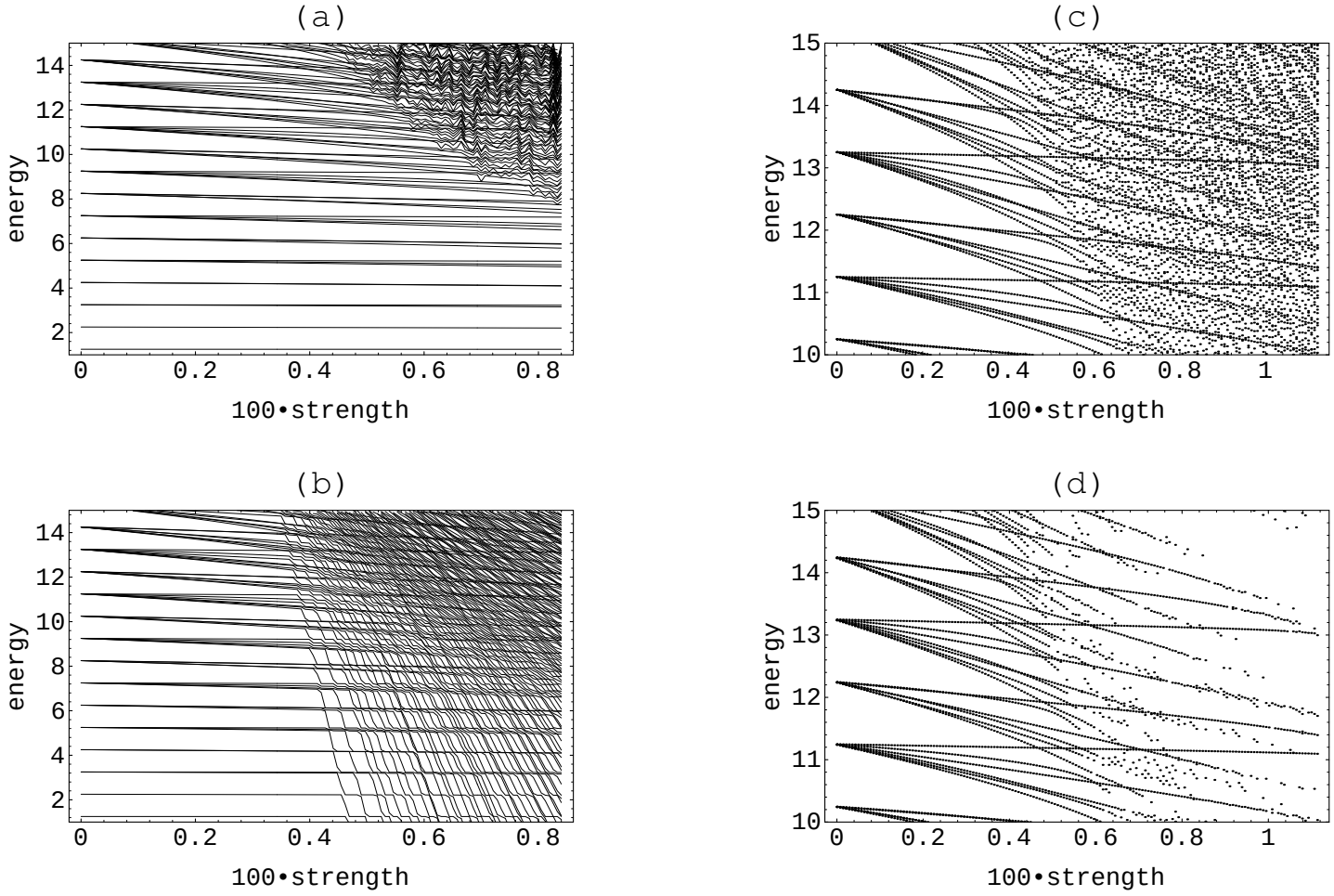
(a)
energy
14
12
10
8
6
4
2
0
0.2
0.4
0.6
0.8
100•strength
(c)
energy
15
14
13
12
11
10
0
0.2
0.4
0.6
0.8
1
100•strength
(b)
energy
14
12
10
8
6
4
2
0
0.2
0.4
0.6
0.8
100•strength
(d)
energy
15
14
13
12
11
10
0
0.2
0.4
0.6
0.8
1
100•strength